HAL open science

Microwave response of coplanar waveguide based on electrodeposited CoFe2O4 nanowires

N. Labchir, A. Hannour, A. Ait Hssi, D. Vincent, J.P. Chatelon, D. Dufeu, A. Ihlal, M. Sajieddine

▶ **To cite this version:**

N. Labchir, A. Hannour, A. Ait Hssi, D. Vincent, J.P. Chatelon, et al.. Microwave response of coplanar waveguide based on electrodeposited CoFe2O4 nanowires. Journal of Magnetism and Magnetic Materials, 2020, 510, pp.166952. 10.1016/j.jmmm.2020.166952 . hal-02944204

HAL Id: hal-02944204

https://hal.science/hal-02944204v1

Submitted on 22 Aug 2022

HAL is a multi-disciplinary open access archive for the deposit and dissemination of scientific research documents, whether they are published or not. The documents may come from teaching and research institutions in France or abroad, or from public or private research centers.

L'archive ouverte pluridisciplinaire **HAL**, est destinée au dépôt et à la diffusion de documents scientifiques de niveau recherche, publiés ou non, émanant des établissements d'enseignement et de recherche français ou étrangers, des laboratoires publics ou privés.

Distributed under a Creative Commons Attribution - NonCommercial 4.0 International License

Version of Record: https://www.sciencedirect.com/science/article/pii/S0304885320301256
Manuscript_f3f71f559bd06a5c5291fa2a332171af

Microwave response of coplanar waveguide based on electrodeposited $CoFe_2O_4$ nanowires

N. Labchir [a,b*], A. Hannour [b], A. A. Hssi[b], D. Vincent [b], J. P. Chatelon [a], D. Dufeu [d], A. Ihlal [b], and M. Sajieddine [c]

[a] *Univ Lyon, UJM-Saint-Etienne, CNRS, LabHC, UMR 5516, F-4203, Saint-Étienne, France*

[b] *Univ Ibn Zohr, Faculty of Sciences Agadir, LabMER, BP 8106, Agadir, Morocco*

[c] *Univ Sultan Moulay Slimane, FST, Materials Physics Laboratory, Béni Mellal, Morocco*

[d] *Institut NEEL CNRS/UGA UPR2940, Cedex 9 ,Grenoble, France*

* Corresponding author: nabill.labchir@univ-st-etienne.fr

Abstract:

Well-crystallized $CoFe_2O_4$ nanowires are grown by electrodeposition into anodic alumina oxide (AAO) membrane. The XRD and EDS analysis confirmed the synthesis of pure $CoFe_2O_4$ with average grain size ranging from 30 to 22 nm. The SQUID investigations revealed that the nanowires electrodeposited at -1.2 V exhibit a large remanent magnetization and high permanent internal magnetic field along the wire axis. The microwave studies emphasized a gyromagnetic resonance around 42 GHz. In addition, numerical simulations performed by HFSS showed good agreement with experimental results. As a consequence, such electrodeposited nanocomposite is a promising candidate for high-frequency microwave devices.

Keywords: $CoFe_2O_4$ nanowires; electrodeposition; CPW transmission line; gyromagnetic resonance.

© 2020 published by Elsevier. This manuscript is made available under the CC BY NC user license
https://creativecommons.org/licenses/by-nc/4.0/

1. Introduction

Over the last decade, nanowire structures have been widely studied due to their promising properties in technological applications. Ferrimagnetic nanowired composites embedded into nanoporous alumina offer the ability to fabricate non-reciprocal and planar devices at high frequencies (>40 GHz), such as circulators **[1,2]**, isolators **[3,4]**, phase shifters **[5,6]** and absorbers **[7,8]**. These electronic components are exploited in wireless communication, radar and military systems. The most advantages of ferrimagnetic nanowires compared to ferrites used in classical circulators, are a higher resonance frequency (RF) associated with a large saturation magnetization **[9,10]**. In the case of nanowire composites, the high uniaxial anisotropy induces an important internal magnetic field in the absence of an external applied magnetic field **[11]**. As a matter of fact, these self-biased materials were considered an effective way to reduce the microwave devices size and weight. Moreover, radio frequency (RF) parameters have been used to study a variety of microwave structures including stripline **[12,13]**, microstrip **[14-16]** and coplanar waveguide (CPW) **[17-18]**. Therefore, the microwave performance of non-reciprocal components can be enhanced by integrating them with a CPW line. The possibility of designing the circulator using the CPW was first investigated in 1971 by Ogasawara et al. [19]. Moreover, CPW line is especially suitable for the design of magnetic monolithic integrated circuits.

Indeed, these nanowired composites can be synthetized at room temperature using low cost techniques, such as electrochemical deposition **[20,21]**. The electrochemical growth of $CoFe_2O_4$ nanowires is affected by many experimental parameters, and the variation of each parameter will change the microstructure and the chemical composition. Therefore, it is necessary to examine the effect of the experimental parameters, such as the deposition potential, in order to improve the magnetic properties of the $CoFe_2O_4$ nanowires.

In the present work, we have fabricated and characterized the anodic alumina oxide (AAO) membrane substrate filled with $CoFe_2O_4$ crystallites. Highly ordered $CoFe_2O_4$ nanowires are elaborated by electrochemical deposition. Their electrochemical growth evolution, morphological, elementary composition, magnetic and microwave properties have been investigated.

2. Experimental

In this work, AAO membranes from Sigma Aldrich company, with a porosity of 50 %, pore diameter of 100 nm and inter pore spacing of 120 nm are used for nanowires growth (**Fig.1**) **[22]**. Prior to electrochemical deposition, a thin layer of copper about 3 µm was sputtered on one back side of the AAO membrane to serve as the working electrode during the growth process. The electrodeposition of $CoFe_2O_4$ nanowires were performed in a three electrode setup controlled by a potentiostat (PGZ 301, Voltamaster 4). The Ag/AgCl electrode was used as reference electrode and a platinum sheet served as counter electrode. The typical fresh aqueous solution is composed of 0.04 M of $CoSO_4.7H_2O$ (98%, Sigma Aldrich), 0.06 M of $FeSO_4.7H_2O$ (99%, Sigma Aldrich), 0.12 M of $(NH_4)_2SO_4$ (99%, Sigma Aldrich) and 0.3 M of H_3BO_3 (99%, Sigma Aldrich). The solution concentrations was adjusted and optimized to get 1:2 atomic composition of Co and Fe. Moreover, a 0.006 M of sulfuric acid (H_2SO_4) was added to the aqueous solution in order to adjust the pH at 3.4, which is the optimal value to avoid the precipitation of Co-Fe alloy onto AAO membrane surface. All chemical products have analytical purity and have been used as received. For the electrodeposition of Co-Fe composite at room temperature, the potential was kept at -1, -1.1 and -1.2 V versus Ag/AgCl.

Fig. 1 (Here)

On the other hand, the microstructure characterization was examined by X'Pert PRO X-ray diffractometer (λ_{Cu} = 1.5406 Å) in the angular range 15-82°. Then, the morphology and the chemical composition of the deposited nanowires was evaluated by Quanta 200-FEI scanning electron microscope (SEM) operating at 10 kV, equipped with energy-dispersive X-ray detector. Moreover, the magnetic and the roughness investigations were achieved by a super quantum interface device (SQUID) magnetometer and Agilent 5500LS atomic force microscope (AFM). In addition, the transmission parameters and the resonance frequency of coplanar waveguide (CPW) line etched on the surface of the $CoFe_2O_4$ nanocomposite were investigated using a RS ZVA67 vector network analyzer (VNA).

3. Results and discussion

3.1 Cyclic voltammetry (CV) and Chronoamperometry (CA)

Cyclic voltammetry (CV) was performed in a range of -1 to -1.2 V vs Ag/AgCl at room temperature for AAO template immersed in a solution containing iron and cobalt ions at scanning rate of 30 $mV.s^{-1}$. The reduction potential of Co-Fe composite into AAO membrane can be determined according to the voltammogram displayed in **Fig. 2**. It was observed that the reduction of active species (Co^{2+} and Fe^{2+} ions) in the electrolyte occurred at about -0.2 V. At this potential, the electrochemical growth of Co-Fe alloy is controlled by electron transfer phenomena. Then, the resulting current density increased slowly until potential -0.7 V indicating the dominance of a mixed control process, which leads to the formation and growth of more Co-Fe composite into the AAO membrane. Thus, a potential plateau region between -1.1 and -1.2 V indicating the deposition of Co-Fe in the pores has been observed. The scanning potential was stopped at -1.4 V due to the hydrogen evolution. Indeed, in the case of an applied potential more than -1.3 V, a large bubble appeared on the AAO membrane surface which can significantly affect the filling of the pores by the Co-Fe composite. As a matter of fact, in order to deposit the Co-Fe composite into AAO templates without hydrogen bubble generation, it is necessary to choose a potential reduction ranging from -1 V to -1.2 V.

Fig. 2 (Here)

Fig. 3 displays the CA current density obtained during the deposition of Co-Fe composite into AAO membrane at various applied potentials for 40 min.

Fig. 3 (Here)

It was observed at the beginning of electrochemical growth that a non-faradaic process involves. In the case of this phenomenon, known as double layer charging (DLC), the Co and Fe ions were arranged at the bottom of membrane pores **[23]**. Next, a stable faradaic current flows after 5 min, and a newly formed phase appears, indicating the growth and the nucleation of Co-Fe in the nanopores under diffusion controlled reaction. From the CA curves, the current density was clearly increased negatively with increasing the applied deposition potential which confirms the enhancement of nucleation efficiency of Co-Fe composite. In this context, a good reproducibility is showed in the different electrodeposition experiments. After this first deposition step, all the electrodeposited samples were annealed at 500 °C in air

for 24 h in order to obtain the phase-pure spinel $CoFe_2O_4$ and also to keep the AAO membrane more thermally stable and avoid any kind of deformation or fragility.

The formation of $CoFe_2O_4$ inside the AAO template is governed by the following reaction:

$$\mathbf{Co^{2+} + 2Fe^{2+} + 8OH^{-} \rightarrow CoFe_2O_4 + 4H_2O + 2e^{-}} \quad (1)$$

3.2 XRD investigations

The crystalline structure of the $CoFe_2O_4$ nanowires electrodeposited at various potentials was explored by XRD (**Fig. 4**).

Fig. 4 (Here)

The XRD spectra suggest that all the prepared nanowires possess a spinel phase, confirming the formation of $CoFe_2O_4$ into the AAO membrane according to the JCPDS standard data (n° 22-1086). The XRD patterns revealed that the all nanowires exhibited a partial orientation along all the reflections. However, we can note the appearance of new peak at 79.8° for $CoFe_2O_4$ deposited at -1.1 V. Furthermore, for the sample electrodeposited at -1.2 V, the XRD spectra emphasized the birth of two new peaks at 71.62 and 37.36° corresponding to spinel $CoFe_2O_4$ phase **[24]**. The cell parameters were determined by a refinement procedure using Fullprof software of all major peaks. As a consequence, the cell parameter (**a**) was found to be 8.32 Å, 8.33 Å and 8.38 Å nm for the nanowires electrodeposited at -1,-1.1 and -1.2 V, respectively. Indeed, the obtained value are in good agreement with that corresponds to $CoFe_2O_4$ single-crystals (a = 8.394 Å) **[25]**.

The significance of the full width at half maximum (FWHM) $\boldsymbol{\delta_{hkl}}$ of peaks evidences crystallite refinement along with the large strain associated with the $CoFe_2O_4$ crystal. The instrumental FWHM was corrected, corresponding to each XRD diffraction peak of the $CoFe_2O_4$ nanocomposite using the following expression:
:

$$\boldsymbol{\delta_{hkl}} = \sqrt{(\boldsymbol{\delta_{hkl}})^2{}_{\text{Measured}} - (\boldsymbol{\delta_{hkl}})^2{}_{\text{Instrumental}}} \quad (2)$$

The average crystallite size (D) for $CoFe_2O_4$ is also calculated from XRD data using the Scherrer formula **[26]**:

$$D = \frac{0.9\lambda}{\delta_{hkl} \cos \theta} \quad (3)$$

where λ is the wavelength of X-ray beam, θ is the Bragg's angle of diffraction.

The results revealed that the crystallite size (D) of the $CoFe_2O_4$ nanocomposite depends on the applied potential. The average crystallite size decreases from 30 to 22 nm for the applied potentials of -1 and -1.2 V, respectively. Moreover, the XRD results show globally that the degree of crystallinity is improved as the applied potential becomes more negative. The evolution of lattice parameter and grain size is explained by the fact that agglomerations of crystallites become smaller by varying the applied potential from -1 to -1.2 V. Similar results are reported recently by A. Franco et al. **[27]**.

3.3 Morphology and chemical composition of $CoFe_2O_4$ nanowires

Fig. 5 shows SEM images evaluating the effect of potential variation on the morphology and the ratio of pore-filling. Prior to the analysis, the back side of the AAO membrane was placed 2 min in the perchloride iron solution in order to remove the copper layer that served as a cathode. Then, the AAO membrane is immersed for 30 min in a solution containing 1 M NaOH to dissolve the alumina and to make $CoFe_2O_4$ nanowires more visible during SEM investigations.

Fig. 5 (Here)

As shown in **Fig. 5** (**a**), (**b**) and (**c**), the pore-filling ratio strongly depends on the deposition voltage. The **Fig. 5(c)** reveals that a total and uniform pore-filling with $CoFe_2O_4$ is obtained at -1.2 V, unlike the samples deposited at -1 and -1.1 V that contain a collection of unfilled pores as observed in **Fig 5 (a)**, and (**b**). This change in pore-filling ratio arises from many phenomena that have occurred during the electrochemical reduction of metal ions into the AAO membrane. However, the thickness reduction of diffusion layer where the ions dynamic is controlled, can drastically change the kinetics of ions diffused from the solution to the pores, thus modifying the nucleation and the growth rate. Consequently, the structure and the composition of the $CoFe_2O_4$ showed a noticeable modification. The diameter of the prepared nanowires is ranging from 100 to 110 nm, which is equivalent to the diameter of the AAO membrane pores. In addition, the elementary composition of the synthetized nanowires,

investigated by the EDS analysis (**Fig. 5**), confirms that no relevant impurities are detected in the $CoFe_2O_4$ nanowires.

Moreover, the EDS analysis (see the tables inserted in Figure 5) reveals better stoichiometry of the $CoFe_2O_4$ nanowires with 15.1% -Co, 28.6% -Fe and 56.3% -O obtained with an applied potential of -1.2 V. This result indicates the good arrangement of the Co, Fe, O cations in the tetrahedral and octahedral sites of the elementary lattice of $CoFe_2O_4$ and confirms the good formation of the spinel phase for the $CoFe_2O_4$ nanowires. In addition, this obtained stoichiometry degree reconfirms the birth of the new peaks observed in the XRD spectrum for a pure spinel phase.

3.4 Surface roughness behavior of nanowires

As shown in **Fig. 6**, the AFM probing technique was used to characterize the topography of $CoFe_2O_4$ nanowires prepared by electrodeposition at various applied potentials**.**

Fig. 6 (Here)

The 2D AFM images are recorded in tapping mode in order to determine the surface roughness of nanowires. The AFM images of $CoFe_2O_4$ nanowires deposited at -1 and -1.1 V confirms clearly the non-filling of the pores. The surface for both samples is typically rough and its roughness is estimated to be about 392 and 350 nm, respectively. Moreover, the surface of nanowires deposited at -1.2 V shows a total filling of the pores. The surface roughness is measured to be about 92.3 nm, which make this surface very homogeneous, compact and also a good candidate for copper sputtering in order to carry out a CPW line.

3.5 SQUID measurements

The magnetic properties of the $CoFe_2O_4$ nanowire arrays performed at different deposition potentials have been measured at room temperature under an applied field up to 1500 kA/m. **Fig. 7** displays the variation of squareness ratio $\frac{\mathbf{M}}{\mathbf{M_s}}$ as a function of applied field H.

Fig. 7 (Here)

Table.1 (Here)

Their corresponding magnetic parameters are listed in Table 1. We have investigated the evolution of the magnetic properties of $CoFe_2O_4$ nanowires arrays as a function of their average chemical composition. Thus, within the composition range between 15 % and 22 % of Co as shown in EDS spectra for the applied potential varying from -1 to -1.2 V, it was found that the nanowires grown at -1.2 V present a great stoichiometry. Moreover, the $CoFe_2O_4$ nanowires electrodeposited at -1.2 V exhibited higher squareness of 0.55 and coercivity H_c of 133 kA/m Oe in parallel direction to wire axis, in comparison to a squareness of 0.46 and coercivity of 130 kA/m in the perpendicular configuration. It is obvious that the squareness and the coercivity are highly affected by the elementary composition of $CoFe_2O_4$ into the AAO membrane. The magnetic response of the $CoFe_2O_4$ nanowires is closely related to the cation distribution in tetrahedral and octahedral sites of spinel phase and also the crystallographic microstructure. Due to the rapid deposition of Fe^{2+} and Co^{2+} into the pores with the variation of the deposition potentials from -1 to -1.2 V, the intrinsic defects and stress increase with the decrease of Co atoms in the nanopores. As a consequence, these factors could improve the crystallographic structure to obtain a pure spinel phase. It has been observed from the hysteresis loops that at -1.2 V, the easy axis is mainly controlled by the shape anisotropy of $CoFe_2O_4$ crystallites into the nanopores. There is a significant diminution in the coercivity parallel and perpendicular to the wire axis when the potential ranges from -1.1 V to -1.2 V. Indeed, this effect is expected due to the decrease in grain size as shown in XRD analysis. Within this context, similar findings have been reported by Ramazani et al. **[28]** for CoFeCu nanowires. Moreover, the internal magnetic field ($\boldsymbol{H_i}$) acting inside the $CoFe_2O_4$ nanowires embedded into AAO template, can be expressed in the remanent state by the following formula **[29]**:

$$\boldsymbol{H_i = H_a - N_z M_s} \tag{4}$$

where $\boldsymbol{H_a}$ the anisotropy field of $CoFe_2O_4$ nanowires, and N is the demagnetizing factor, which is equal to 0 in the case of an elongated magnetic cylinder polarized vertically along z axis.

The $\boldsymbol{H_a}$ value is determined experimentally by the intersection between the edges of the hysteresis cycles in the two measurement directions (parallel and perpendicular) as described in **Fig. 7**. Table 1 summarizes the values collected for $\boldsymbol{H_a}$. As expected, the nanowires elaborated electrochemically at -1.2 V have an anisotropy field of 1.5 T. In this case, the

internal magnetic field $\boldsymbol{H_i}$ of the $CoFe_2O_4$ nanowires is proportional to the anisotropy field, and we can write $\boldsymbol{H_i} \simeq \boldsymbol{H_a}$.

3.6 Microwave characterization

For the microwave behavior, the ferrimagnetic composite used to fabricate the coplanar transmission line is the sample deposited at -1.2 V due to a large internal magnetic field and a minimum roughness emphasized by SQUID and AFM measurements, respectively. The saturation magnetization $(\boldsymbol{M_s})$ for a filled membrane is close to 0.18 T. As a matter of fact, for the $CoFe_2O_4$ nanowires, the M_s value is approximately equal to 0.36 T since the porosity of the AAO template is around 50 %. This value is quite close to this generally attributed to bulk material which is 0.48 T. In addition, an effective permittivity of 11 as the average value between alumina Al_2O_3 and $CoFe_2O_4$ nanowires was introduced into HFSS during the simulations. As shown in **Fig. 8**, the 3D design of the CPW line and the numerical studies at high-frequency are performed using the three dimensional software HFSS based on the finite elements method (FEM).

Fig. 8 (Here)

In the CPW structure, the conductor and the ground planes are placed on the same level on the magnetic composite. In this work, a 72/40 µm (72 µm is the width of conductor and 40 µm is the width of the slot) CPW transmission line was etched in the 3 µm thick copper deposited by RF sputtering on the $CoFe_2O_4$ nanowires surface. The line has been designed for a characteristic impedance of about 50 Ω with 10 mm ~~in~~ length. Two ports are connected to a vector network analyzer (VNA). Open-Short-Through-Load (OSTL) calibration was performed using the picoprobe kit. The measurements were made from 15 to 60 GHz without external magnetic field as shown in **Fig. 9**.

Fig. 9 (Here)

The simulated and measured transmission parameters S_{12} and S_{21} are displayed in **Fig. 10** (**a**). and (**b**), respectively.

Fig. 10 (Here)

For these first measurements (**Fig. 10 (b)**), we obtain a reciprocal (S_{12}=S_{21}) behavior which was expected because the configuration adopted during the microwave measurements does not allow to observe the non-reciprocal effect. More precisely, in our realized structure the internal magnetic field $\boldsymbol{H_i}$ remaining along the $CoFe_2O_4$ nanowires is perpendicular to the electric field existing on the copper lines, which prevents the birth of the field displacement phenomenon. This mentioned effect is responsible for the appearance of the non-reciprocal effect of nanowires **[30]**.

The measurements show significant losses around 41.2 GHz originated from the $CoFe_2O_4$ nanowired composite. We can note a fairly broadband effect due to the gyromagnetic resonance of cobalt ferrite. It is possible to estimate the value of the resonance frequency using the Kittel formula **[9]**:

$$\boldsymbol{2\pi f_{res} = \gamma \mu_0 H_{eff}} \tag{5}$$

with $H_{eff} = H_a - M$

where γ is the gyromagnetic ratio given in GHz by Tesla ($\gamma\mu_0 = 2\pi \times 28\ GHz/T$), and $\boldsymbol{H_{eff}}$ is the effective field inside the material, depending of the anisotropy field and the magnetization $\boldsymbol{M}$. $\boldsymbol{M}$ can be close to the saturation magnetization $\boldsymbol{M_s}$ when the material is sufficiently magnetized.

The calculation gives a resonance frequency close to 39.5 GHz, indicating a permanent internal magnetic field inside the nanowires about 1.5 T. As a matter of fact, the internal field calculus requires the use of a magnetic material complex model taking into account the dispersion of the magnetic domains and moments inside the nanowaires leading to a ratio $\frac{\boldsymbol{M}}{\boldsymbol{M_s}}$ inferior to 1 **[31]**, while the model used in the simulation software is a model for saturated materials (Polder model).

However, this first approach shows results in good agreement with the experimental value deduced from SQUID investigations, may be due the weak value of $\boldsymbol{M}$ compared to $\boldsymbol{H_a}$. The predictions of the S parameters performed by HFSS (**Fig. 10** (**c**)) give us an approximate value of the internal field **[32]**.

4. Conclusion

In summary, we have developed a nanocomposite magnetic material based on cobalt ferrite nanowires synthesized via electrodeposition technique. The XRD and EDS investigations have revealed a good crystallization associated with a higher stoichiometry of the cobalt

ferrite electrodeposited at -1.2 V. Moreover, SQUID and AFM measurements indicated a large internal magnetic field and a better roughness for the nanowires grown at -1.2 V. The microwave response has been performed using a coplanar transmission line etched in a clean room on the surface of the nanowires. This coplanar structure emphasized a gyromagnetic resonance frequency around 42 GHz, thus indicating a strong anisotropy field of 1.5 T and the possibility of using this nanocomposite in millimetric band. In addition, the simplicity of synthesis and the low annealing temperature (500 °C) make it an attractive candidate for the design of non-reciprocal components.

Acknowledgments

The authors acknowledge the financial support of PHC-Toubkal under the project TBK/85/17, Campus France: 38983UH.

References

[1] J. Kerckhoff, K. Lalumière, B. J. Chapman, A. Blais, and K. W. Lehnert, On-chip superconducting microwave circulator from synthetic rotation. Phys. Rev. Appl, 4(3) (2015) 034002.

[2] N. Labchir, A. Hannour, D. Vincent, A. Ihlal, and M. Sajieddine, Magnetic Field Effect on Electrodeposition of $CoFe_2O_4$ Nanowires, Appl. Phys. A. 125(11) (2019) 748.

[3] S. Chen, C. Zhao, Y. Li, H. Huang, S. Lu, H. Zhang, and S. Wen. Broadband optical and microwave nonlinear response in topological insulator. Opt. Mater. Express, 4(4) (2014) 587-596.

[4] C. W. Peterson, W. A. Benalcazar, T. L. Hughes, and G. Bahl, A quantized microwave quadrupole insulator with topologically protected corner states. Nature, 555 (7696) (2018) 346.

[5] Y. Zhang, and S. Pan. Broadband, Microwave signal processing enabled by polarization-based photonic microwave phase shifters. IEEE J. Quantum. Electron. 54(4) (2018) 1-12.

[6] V. K. Palukuru, J. Peräntie, J. Jäntti, and H. Jantunen, Tunable microwave phase shifters using LTCC technology with integrated BST thick films. Int. J. Appl. Ceram. Tec. 9(1) (2012)11-17.

[7] L. Qiao, X. Han, B. Gao, J. Wang, F. Wen, and F. Li, Microwave absorption properties of the hierarchically branched Ni nanowire composites. J. Appl. Phys. 105(5) (2009) 053911.

[8] W. Chen, M. Han, and L. Deng, High frequency microwave absorbing properties of cobalt nanowires with transverse magnetocrystalline anisotropy. Physica B: Condens. Matter. 405(6) (2010) 1484-1488.

[9] A. Hannour, D. Vincent, F. Kahlouche, A. Tchangoulian, S. Neveu, and V. Dupuis, Self-biased cobalt ferrite nanocomposites for microwave applications. J. Magn. Magn. Mater. 353 (2014) 29-33.

[10] V. Sharma, B. K. Kuanr, and Z. Celinski, Microwave Monolithic Devices Using Magnetic Hard-Soft Nanocomposite. *IEEE. Trans. Magn*. 55(7) (2019) 1-4.

[11] A. Encinas, M. Demand, L. Vila, L. Piraux, and I. Huynen, Tunable remanent state resonance frequency in arrays of magnetic nanowires. Appl. Phys. Lett. 81(11) (2002) 2032-2034.

[12] S. S. Kalarickal, P. Krivosik, M. Wu, and C. E. Patton, Ferromagnetic resonance linewidth in metallic thin films: Comparison of measurement methods. J. Appl. Phys. 99 (2006) 1-7.

[13] I. S. Maksymov, and M. Kostylev, Broadband Stripline Ferromagnetic Resonance Spectroscopy of Ferromagnetic Films, Multilayers and Nanostructures. Physica E. 69 (2015) 252-293.

[14] R. Ramirez-Villegas, I. Huynen, L. Piraux, A. Encinas, and J. De La Torre Medina , Configurable Microwave Filter for Signal Processing Based on Arrays of Bistable Magnetic Nanowires. IEEE. Trans. Microw. Theory. Tech. 65 (2017) 72-77.

[15] M. Sharma, B. Kuanr, M. Sharma, and A. Basu, New Opportunities in Microwave Electronics with Ferromagnetic Nanowires. J. Appl. Phys, 115 (2014) 1-3.

[16] H. W. Yao, A. Abdelmonem, J. F. Liang, and K. A. Zaki, Analysis and design of microstrip to-waveguide transitions. IEEE. Trans. Microw. Theory. Tech. 42(12) (1994) 2371-2380.

[17] C. Bilzer, T. Devolder, P. Crozat, C. Chappert, S. Cardoso, and P. P. Freitas, Vector Network Analyzer Ferromagnetic Resonance of Thin Films on Coplanar Waveguides: Comparison of Different Evaluation Methods. J. Appl. Phys, 101 (2007) 1-5.

[18] Y. Endo, Y. Shimata, and M. Yamaguchi, Study on the Magnetization Dynamics of Ni–Fe Dot Arrays Estimated by the CPW-FMR Measurement Method. IEEE. Trans. .Magn 51 (2015) 3517-3519.

[19] N. Ogasawara and M. Kaji, Coplanar-guide and slot-guide junction circulators. *Electron. Lett*. 7(9) (1971) 220-221.

[20] N. Labchir, A. Hannour, D. Vincent, A. A. Hssi, A. Ihlal, and M. Sajieddine, Magneto-electrodeposition of granular Co–Cu nanowire arrays. Mater. Res. Express. 6(11) (2019) 1150c3.

[21] A. Ait hssi, L. Atourki, N. Labchir, M. Ouafi, K. Abouabassi, A. Elfanaoui, A. Ihlal, and K. Bouabid, Optical and dielectric properties of electrochemically deposited p-Cu2O films. Mater. Res. Express. (2020) 1-7, doi: 10.1088/2053-1591/ab6772

[22] Z. L. Xiao, C. Y. Han, U. Welp, H. H. Wang, W. K. Kwok, G. A.Willing, and G. W. Crabtree, Fabrication of alumina nanotubes and nanowires by etching porous alumina membranes. Nano Letters, 2(11) (2002) 1293-1297.

[23] M. S. Kilic, M. Z. Bazant, and A. Ajdari, Steric effects in the dynamics of electrolytes at large applied voltages. I. Double-layer charging. Phys. Rev. E. 75(2) (2007) 021502.

[24] S. Mitra, P. S. Veluri, A. Chakraborthy, and R. K. Petla, Electrochemical properties of spinel cobalt ferrite nanoparticles with sodium alginate as interactive binder. Chem. Electro. Chem. 1(6) (2014) 1068-1074.

[25] N. Labchir, A. Hannour, D. Vincent, A.A. Hssi, M. Ouafi, K. Abouabassi, A. Ihlal, and M. Sajieddine, Tailoring the Optical Bandgap of Pulse Electrodeposited $CoFe_2O_4$ Thin Films, J. Electron. Mater. (2020) 1-7, doi 10.1007/s11664-019-07923-y.

[26] N. Labchir, E. Amaterz, A. Hannour, D. Vincent, A. Ihlal, and M. Sajieddine, Highly Efficient Nanostructured $CoFe_2O_4$ Thin Film Electrodes for Electrochemical Degradation of rhodamine B. Water. Environ. Res. (2019) 1-7, https://doi.org/10.1002/wer.1272.

[27] A. Franco, F. L. A. Machado, and V. S. Zapf, Magnetic properties of nanoparticles of cobalt ferrite at high magnetic field. J. Appl. Phys, 110(5) (2011) 053913.

[28] A. Ramazani, M. A. Kashi, F. Eghbal, and E. Jafari-Khamse, The effect of deposition parameters on the magnetic behavior of CoFe/Cu multilayer nanowires. Eur. Phys. J. B, 130(1) (2015) 2.

[29] V. Laur, G. Vérissimo, P. Quéffélec, L. A. Farhat, H. Alaaeddine, E. Laroche, and J. P. Ganne, Self-biased Y-junction circulators using lanthanum-and cobalt-substituted strontium hexaferrites. IEEE. Trans. Microw. Theory. Tech. *63*(12) (2015) 4376-4381.

[30] S. Kirouane, E. Verney, D. Vincent, and A. Chaabi, Simulation results on a new non symmetrical coplanar isolator structure using magnetic thin film. PROG. Electromagn. Res. 8 (2009) 161-170.

[31] V. Boucher, L. P. Carignan, T. Kodera, C. Caloz, A. Yelon, and D. Ménard, Effective permeability tensor and double resonance of interacting bistable ferromagnetic nanowires. Phys. Rev. B, 80(22) (2009) 224402.

[32] B. K. Kuanr, V. Veerakumar, R. Marson, S. R. Mishra, R. E. Camley, and Z. Celinski, Nonreciprocal microwave devices based on magnetic nanowires. Appl. Phys. Lett. 94(20) (2009) 202505.

Figure captions:

Fig. 1. SEM images of AAO membrane: (a) top view, (b) cross sectional view.

Fig. 2. Voltammogram of electrolyte containing 0.04 M CoSO4, 0.06 M of FeSO4 and 0.12 M of $(NH4)_2SO4$ and 0.3 M of H_3BO_3. The scanning rate is 30 mV/s.

Fig. 3. Chronoamperometric curves of electrochemical reduction of Co-Fe alloy into nanoporous AAO membrane at different constant potential of -1 V, - 1.1 V and -1.2 V for 40 min.

Fig. 4 XRD patterns of $CoFe_2O_4$ nanowires electrodeposited into AAO membrane.

Fig. 5 SEM images and corresponding EDS spectra of $CoFe_2O_4$ nanowires electrodeposited at various potentials: (a) -1V, b) -1.1 V and c) -1.2 V.

Fig. 6 2D AFM images of deposited $CoFe_2O_4$ nanowires at -1 V (a), -1.1 V (b) and -1.2 V (c).

Fig. 7 Hysteresis loops of $CoFe_2O_4$ nanowire arrays grown at different deposition potentials.

Fig. 8 Designed coplanar waveguide (CPW) in HFSS software.

Fig. 9 Characterization of coplanar waveguide fabricated on the $CoFe_2O_4$ nanowire surface.

Fig. 10 Simulated and measured forward S_{12} and reverse S_{21} transmissions of $CoFe_2O_4$ nanowires: (a) HFSS simulations, b) VNA measurements, c) comparison between HFSS and VNA results.

Table captions:

Table.1 Magnetic parameters of $CoFe_2O_4$ nanowires deduced from SQUID measurements

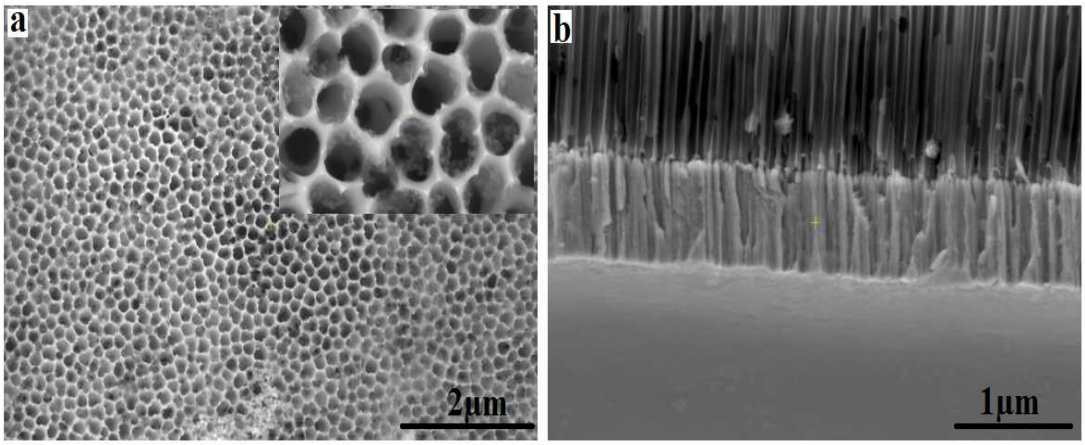

Fig. 1

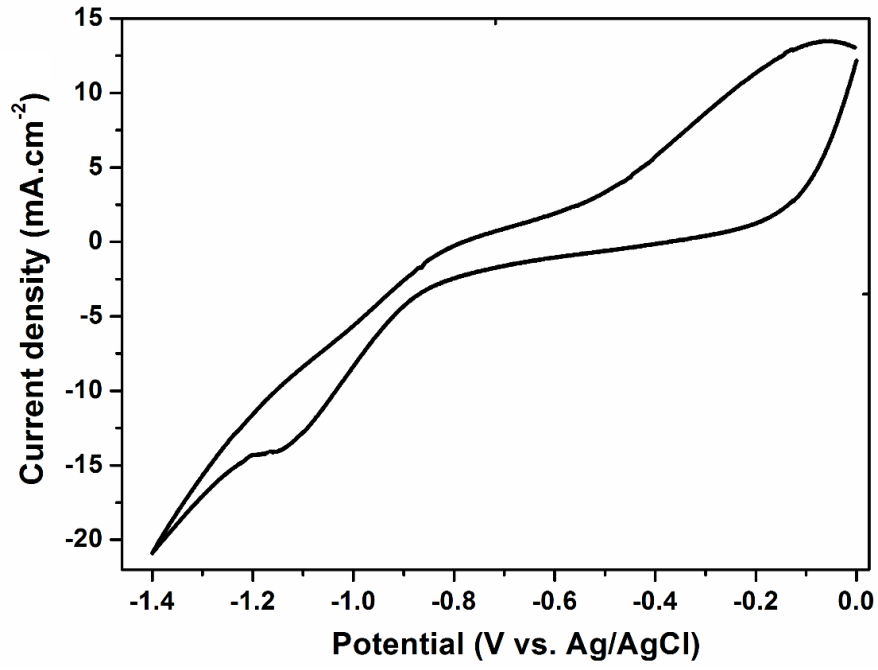
15
10
5
0
-5
-10
-15
-20
Current density (mA.cm-2)
-1.4
-1.2
-1.0
-0.8
-0.6
-0.4
-0.2
0.0
Potential (V vs. Ag/AgCl)

Fig. 2

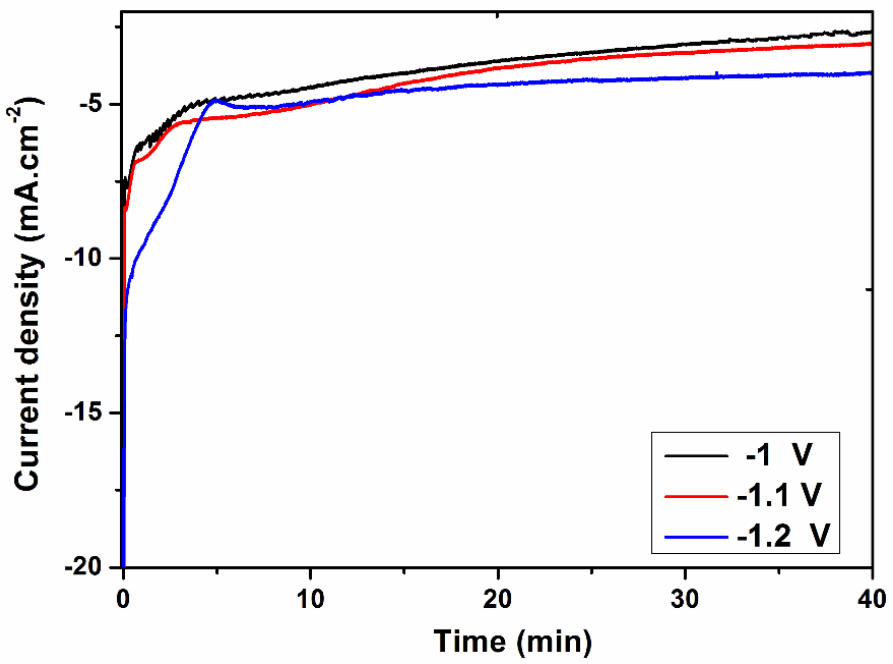
Current density (mA.cm^{-2})
-5
-10
-15
-20
0
10
20
30
40
Time (min)
-1 V
-1.1 V
-1.2 V

Fig. 3

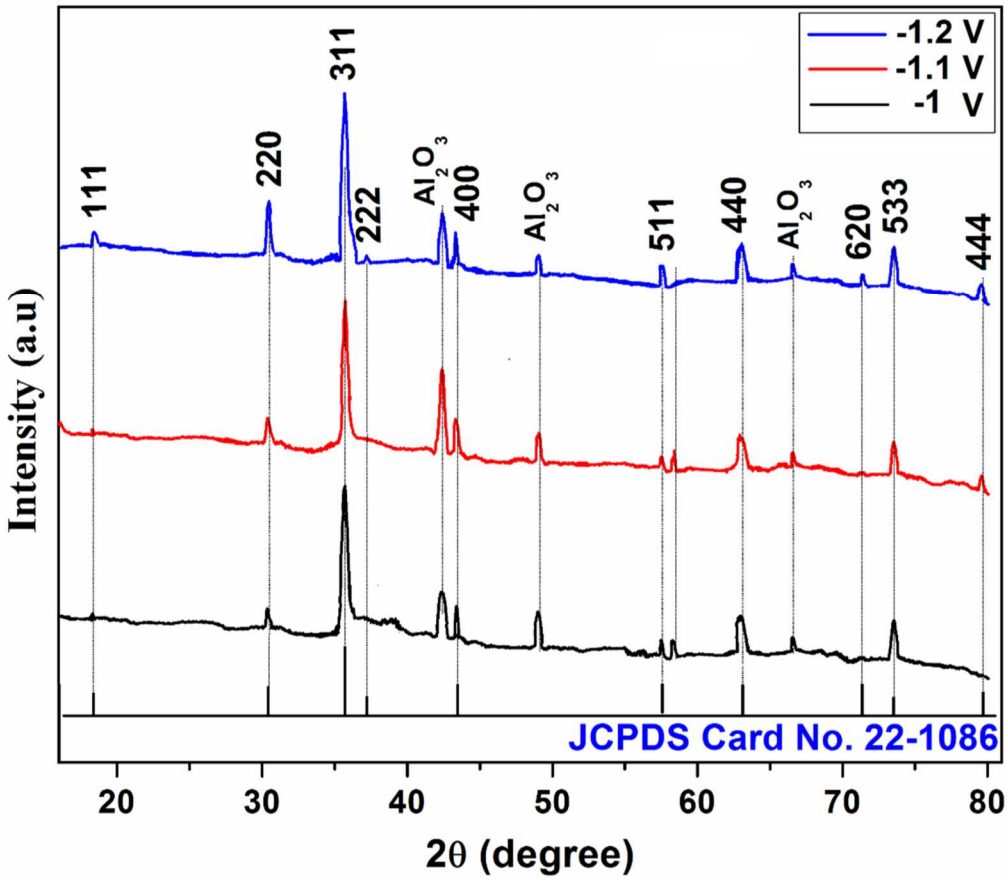
-1.2 V
-1.1 V
-1 V
111
220
311
222
Al2O3
400
Al2O3
511
440
Al2O3
620
533
444
Intensity (a.u)
JCPDS Card No. 22-1086
20
30
40
50
60
70
80
2θ (degree)

Fig. 4

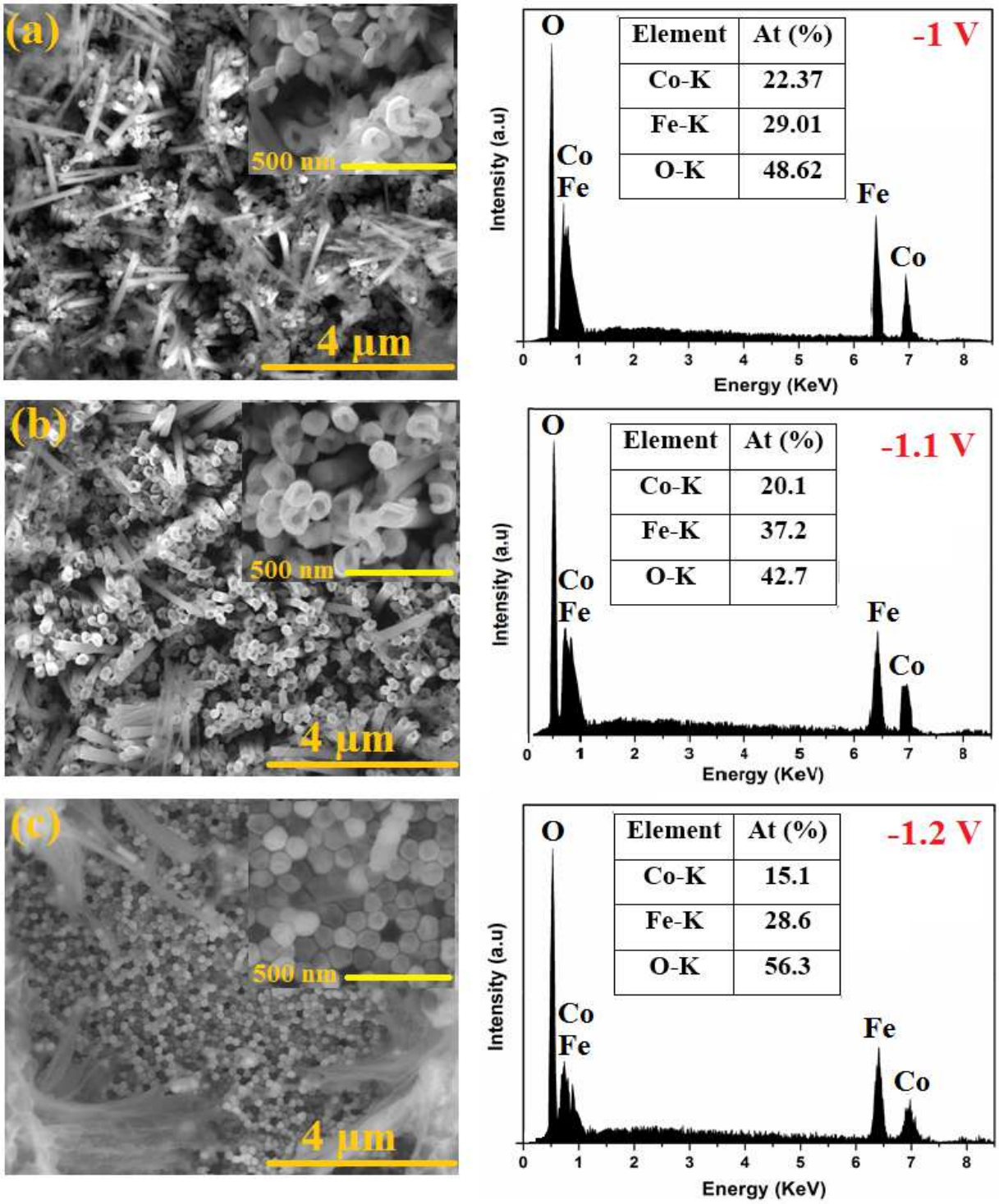

Element	At (%)
Co-K	22.37
Fe-K	29.01
O-K	48.62

Element	At (%)
Co-K	20.1
Fe-K	37.2
O-K	42.7

Element	At (%)
Co-K	15.1
Fe-K	28.6
O-K	56.3

Fig. 5

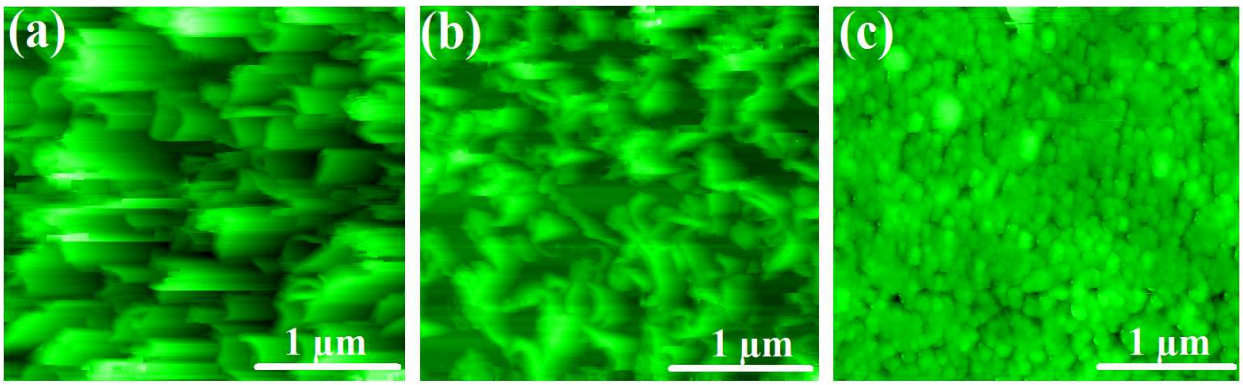

Fig. 6

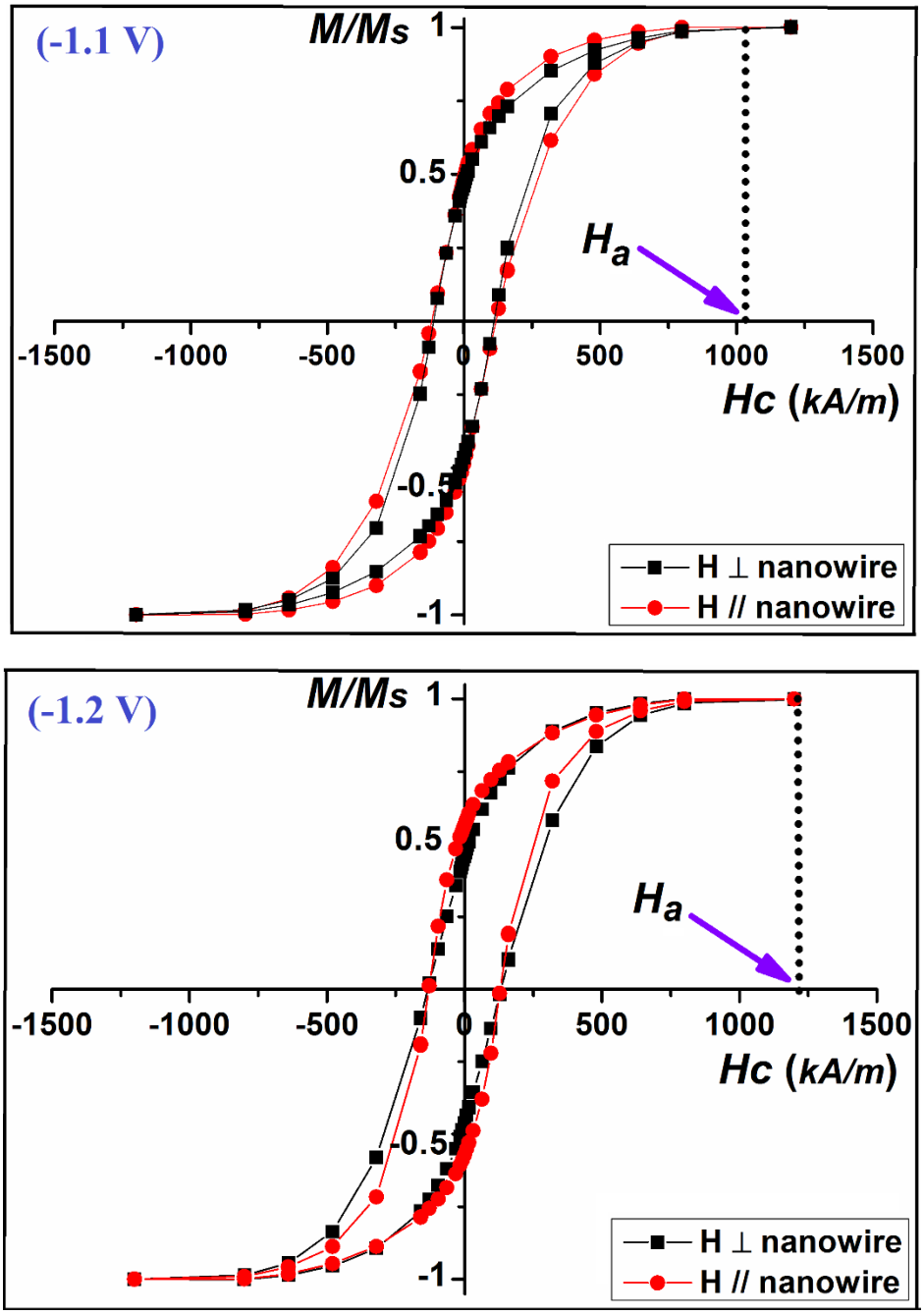
(-1.1 V)
M/Ms
1
0.5
-0.5
-1
-1500
-1000
-500
0
500
1000
1500
Hc (kA/m)
Ha
H ⊥ nanowire
H // nanowire
(-1.2 V)
M/Ms
1
0.5
-0.5
-1
-1500
-1000
-500
0
500
1000
1500
Hc (kA/m)
Ha
H ⊥ nanowire
H // nanowire

Fig. 7

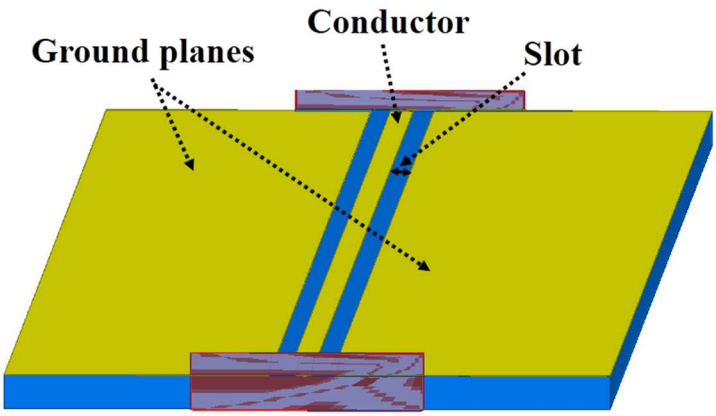

Fig. 8

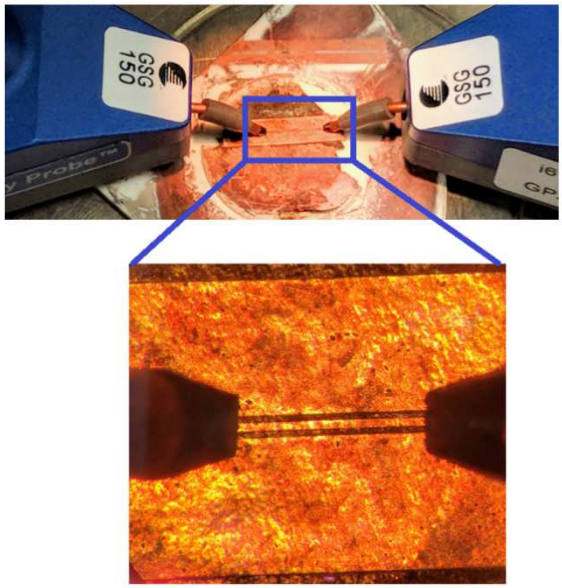

Fig. 9

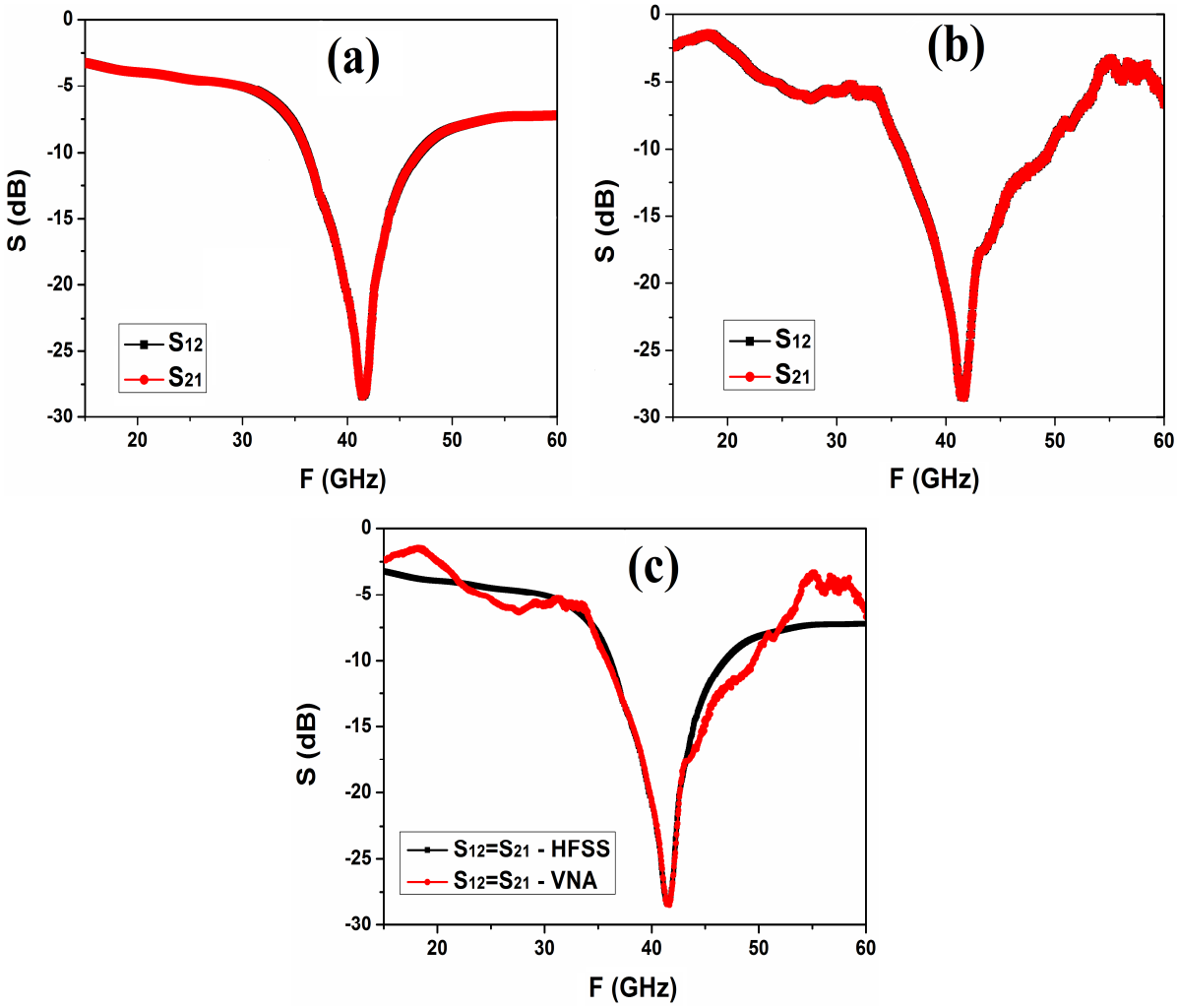
(a)
S (dB)
F (GHz)
S12
S21
(b)
S (dB)
F (GHz)
S12
S21
(c)
S (dB)
F (GHz)
S12=S21 - HFSS
S12=S21 - VNA

Fig. 10

Magnetic parameters / *Deposition potential*	*// nanowires*		*⊥ nanowires*		*Anisotropy field*
	$\frac{M}{M_s}$	H_c (kA/m)	$\frac{M}{M_s}$	H_c (kA/m)	H_a (T)
-1.1 V	*0.49*	*117*	*0.44*	*110*	*1.25*
-1.2 V	*0.55*	*133*	*0.46*	*130*	*1.5*

Table. 1